Direct comparison between Co-28Cr-6Mo alloy prepared by Selective Laser Melting and traditional investment casting

M Roudnicka[1,2], J Bigas[1], V Sreibr[3], D Palousek[3] and D Vojtech[1]

[1]Department of Metals and Corrosion Engineering, University of Chemistry and technology Prague, Technicka 5, 166 28 Prague 6, Czech Republic

[2]FZU – Institute of Physics of the Czech Academy of Sciences, Na Slovance 1999/2, 182 21 Prague 8, Czech Republic

[3]Institute of Machine and Industrial Design, Brno University of Technology, Technicka 2896/2, 616 69 Brno, Czech Republic

E-mail: michaela.roudnicka@vscht.cz

Abstract. Thanks to high mechanical properties stable at elevated temperatures, high abrasion resistance, suitable corrosion resistance and biocompatibility, ternary cobalt alloy Co-28Cr-6Mo is a widely used material in the field of aviation industry and medical implants production. Due to the difficult formability and machinability of this alloy in combination with complex shapes of produced parts, investment casting is the mostly employed production process. However, additive manufacturing provides new processing opportunities. E.g. Selective Laser Melting (SLM) technology fusing metallic powders by precisely focused and controlled laser beam enables the production of highly complex parts with high precision. In this contribution, we bring a direct comparison between the microstructures and mechanical properties of Co-28Cr-6Mo alloy prepared by SLM and investment casting. Due to significant differences in microstructure fineness and phase composition, SLM is revealed to increase not only material strength and hardness but concurrently plasticity. As a result of rapid solidification during SLM, very fine cellular microstructure with Mo microsegregation at cell walls is formed without the occurrence of any secondary phases. The distinctive microstructure of the additively manufactured alloy can be expected to be the cause of many other variances in the material behaviour.

1 Introduction

Due to bad machinability, formability and weldability, cobalt-chrome alloys are mostly processed by casting. From the time and economic point of view, casting is the best solution, especially in case of investment casting which yields products of final shapes with a good surface condition. Only minor finishing operations are thus necessary. However, lower material performance is usually obtained by casting compared to different production techniques, such as forming or powder metallurgy, which limits some demanding applications [1].

New opportunities have been brought by the implementation of additive manufacturing (AM) into the processing of cobalt-chrome alloys. Powder-based techniques of AM, such as Selective Laser Melting (SLM) or Electron Beam Melting (EBM), enable direct production of complex-shaped parts with high precision thanks to the successive processing of small amounts of fine powders by a

precisely focused energy beam. In addition, they offer other benefits highly valued by high-performance applications in the fields as aviation industry or medical implants production. E.g. the possibility of topology optimization and introduction of porous structures may significantly reduce the weight of aircraft parts and thus reduce fuel consumption and operating costs or bring better fixation and thus longevity of bone implants [2, 3].
The ternary Co-28Cr-6Mo alloy is one of cobalt-chrome alloys frequently applied for such applications, e.g. knee and hip arthroplasty or gas turbine parts [4]. Therefore, this paper is focused on its processing by AM, specifically by SLM, and comparison with parts produced conventionally by investment casting. Although several papers have been published on the SLM of this alloy, only a few show directly the comparison between completely different microstructures and the effect of such difference on mechanical performance [5]. Understanding the difference is a prerequisite for extensive testing of many other material manifestations that can crucially influence the confidence of potential part operation. More background data are thus desirable.

2 Materials and Methods

2.1 Studied materials

The material studied in this work is a Co-28Cr-6Mo alloy conforming to the ASTM F75 standard. To provide a comparison between the microstructure and mechanical properties of this material prepared conventionally by investment casting or prepared by additive manufacturing (AM), commercially available materials have been used. The material produced by investment casting was provided by Prospon s.r.o. company; the exact production parameters are thus not available. In case of AM, a commercially available gas-atomized powder of Co-28Cr-6Mo alloy with a particle size of 10−45 μm was purchased from SLM Solutions and was further processed. The chemical composition given by the producers which conforms to the ASTM F75 standard is given in table 1 together with the exact composition determined by X-ray fluorescence (Axios FAST). The composition of both materials meets the standard. The cast material contains little more admixtures than the AM material.

Table 1. Chemical composition (wt.%) of the Co-28Cr-6Mo alloy.

	Co	Cr	Mo	Si	Mn	Fe	Ni
ASTM F75	bal.	27.0−30.0	5.0−7.0	max. 1.0	max. 1.0	max. 0.75	max. 0.5
cast	bal.	29.4±0.3	5.9±0.1	0.82±0.03	0.69±0.04	0.18±0.03	0.25±0.04
SLM	bal.	28.3±0.30	6.3±0.1	0.41±0.02	0.34±0.03	0.07±0.02	0.17±0.03

Quite surprising founding was provided by the combustion analysis (Bruker G4 Icarus HF) for the determination of C, S, N and O content. The content of these impurities is given in table 2 together with the ASTM F75 prescription. The standard allows relatively high content of C which serves as the main precipitation-strengthening element. However, compared to the cast material, the AM material is almost free of C and S as well. That indicates the impossibility of carbide formation and suggests a different material response to heat treatment. In case of gaseous elements, N and O, the rapidly solidified AM material is more prone to their capture.

Table 2. Impurity content (ppm) in the Co-28Cr-6Mo alloy.

	C	S	N	O
ASTM F75	max. 3500	max. 100	max. 2500	−
cast	2300±130	38±1	245±5	62±3
SLM	70±40	7±2	639±4	345±57

Additive manufacturing via the SLM technology was carried out on an SLM Solutions 280 HL machine with the process parameters set-up given in table 3. Testing samples directly in the shape of round tensile

test specimens (figure 1) were built in the vertical orientation using a stripe scanning strategy. The working chamber was supplied with a nitrogen atmosphere to prevent oxidation. The building plate was preheated to 100 °C.

Table 3. SLM process parameters.

Laser power (W)	Scanning speed (mm s^{-1})	Hatching distance (mm)	Layer thickness (mm)
275	800	0.12	0.05

Figure 1. A testing sample produced by SLM.

2.2 Microstructure characterization

As-polished metallography sections were captured by optical microscopy (OM, Zeiss Axio Lab.A1) and subjected to image analysis (ImageJ) for porosity determination. No porosity was detected in the cast material and the additively manufactured material showed a high relative density too; porosity was 0.03%. Microstructures were etched by aqua regia (31% HCl + 65% HNO_3, 3:1) and observed by OM as well as by a scanning electron microscope (SEM, JEOL JSM-6010PLUS/LA) supplemented by EDS analyser. Phase composition was determined by X-ray diffraction (XRD, PANalytical X'Pert PRO with Cu anode). Grain size was determined by the image analysis of etched longitudinal sections.

2.3 Mechanical testing

On the prepared metallographic sections, Vickers hardness HV10 was measured using a Wilson VH3300 hardness tester. Uniaxial tensile and compressive tests were carried out on a universal loading machine Instron 5882. Constant deformation rate of 0.001 s^{-1} was set for all measurements. Tensile and compressive testing was done only with the load acting in the building direction of the samples. For tensile testing, additively manufactured samples were used directly (figure 1), with polishing the surface to the final diameter of 4.8 mm. For compressive testing, cylinders with a height-to-diameter ratio of 1.5 were prepared by cutting the gauge of the as-built tensile samples.

3 Results and Discussion

3.1 Microstructure of cast Co-28Cr-6Mo alloy

The microstructure of the cast Co-28Cr-6Mo results from a relatively slow melt solidification (tens of °C/min) from the casting temperature of ~ 1550 °C. It is thus formed by coarse (100–1000 μm) equiaxed grains (figure 2a) of dendritic nature. Despite relatively slow cooling, high-temperature FCC γ-phase is retained due to the sluggish nature of γ-FCC → ε-HCP transformation [6]. The proportion of ε-phase depends on the cooling rate; for casting, it is in the order of % units (e.g. 4% in ref. [7]). As this phase is much harder and significantly promotes tribological properties, enhancing its content is desirable for biomedical applications such as joint replacements [6]. That can be achieved by isothermal heat treatment below transformation temperature (~ 970 °C [7]), which was most probably applied on the material obtained for this work. The XRD analysis showed the Co matrix to be formed by the FCC γ-phase from 72% and HCP ε-phase from 28%. López and Saldivar-Garcia [7] reached such content of ε

by annealing at 850 °C for 12 h. The nucleation of ε needles occurs at stacking faults of FCC grains, preferably in the areas where Cr and Mo content are not reduced by carbide formation. Carbides are formed in the interdendritic spaces due to Cr and Mo segregation (figure 2a). Interdendritic carbides are thus situated in FCC areas while needle-like ε-phase fills the areas in between (darker matrix areas).

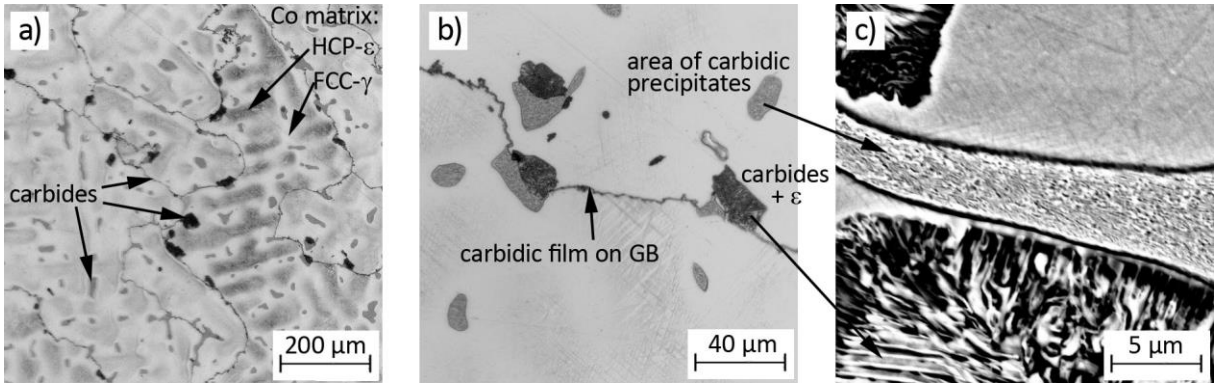

Figure 2. Microstructure of the Co-28Cr-6Mo casting.

XRD proved the presence of $M_{23}C_6$ and M_6C carbides, which contents were determined to be 5.0 and 1.3%. M_6C carbides form mainly a continuous film on grain boundaries (figure 2b). The relatively coarse (10-20 µm) interdendritic carbidic particles are of two different types. Grey carbidic areas (figure 2b) are areas of nanosized precipitates of $M_{23}C_6$ (figure 2c) formed probably by the decomposition of metastable σ-phase below 1150 °C; $\sigma + C \rightarrow M_{23}C_6$ [8]. The XRD analysis did not prove the presence of tetragonal σ-phase; the decomposition was complete. Lesser amount of black carbidic areas closely adjacent to the grey carbide particles (figure 2b) then represents lamellar mixture of carbides and ε-phase formed by the concurrent nucleation of ε-phase and carbide precipitation during isothermal annealing [6]. Table 3 shows the average chemical composition in these carbidic areas in comparison to the composition of the Co-matrix determined by multiple EDS point analyses. The values of C content are only comparative due to the insensibility of EDS to C analysis. The areas of carbide precipitates show the highest content of Mo and Cr.

Table 3. Chemical composition (wt.%) of different areas of the cast Co-28Cr-6Mo alloy.

	Co	Cr	Mo	C	Si
Areas of carbide precipitates	bal.	46.1±1.2	26.1±0.5	7.5±0.5	1.3±0.2
Lamellar mixture of carbides + ε	bal.	40.3±7.4	11.6±3.0	6.3±0.5	0.7±0.1
Co-matrix	bal.	28.4±0.9	6.7±1.4	3.8±1.1	0.8±0.1

3.2 Microstructure of powdered and subsequently additively manufactured Co-28Cr-6Mo alloy

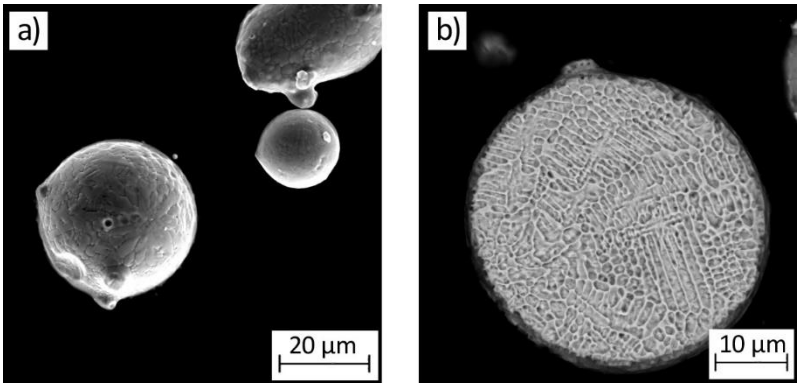

Figure 3. Powder of the Co-28Cr-6Mo alloy for SLM: (a) particle shape, (b) microstructure.

Figure 3 shows the appearance and microstructure of the as-purchased Co-28Cr-6Mo powder prepared by gas atomization. The dendritic structure is visible on the particle surface already (figure 3a). It results from rapid solidification (about 10^4 °C/s [9]) during gas atomization. XRD analysis confirmed that all material is in the state of single FCC γ-phase although microsegregation at interdendritic spaces is obvious from figure 3b. The microsegregation of Mo was confirmed by multiple EDS analyses which showed 7.4±0.9 wt.% of Mo in the interdendritic spaces and 4.9±0.2 wt.% in the dendrites.

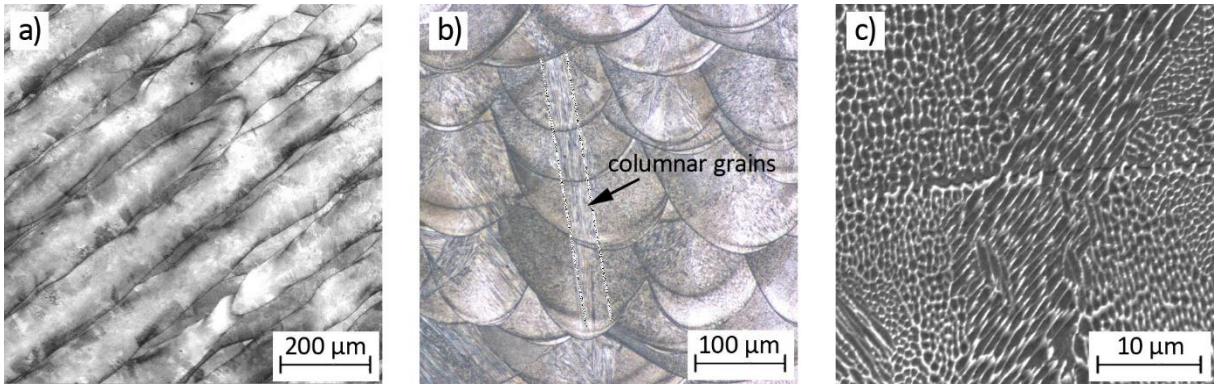

Figure 4. Microstructure of the bulk Co-28Cr-6Mo alloy produced by SLM: (a) cross section, (b) longitudinal section, (c) cellular microstructure.

The bulk material produced by SLM is documented by the images in figure 4. In the first magnification, the characteristic features of layer-by-layer production are visible; single tracks oriented in the scanning direction can be observed in the cross section (figure 4a) while a layered structure of overlapping melt pools is observed in the longitudinal section parallel to the building direction (figure 4b). The depth of the melt pools is approx. double the layer thickness, which ensures proper layers interconnection. Columnar grains sometimes growing across several melt pool depths can be distinguished (figure 4b). The grains of 18±2 µm in thickness can reach length of hundreds of micrometres. Columnar growth is given by the layer-wise production in which already formed grains in a previous layer represent nucleation sites for melt crystallization [10].

The SEM image (figure 4c) shows the cellular microstructure formed due to very high cooling rates during SLM. In each grain, cells show a different orientation. Usually, the crystallographic direction ⟨100⟩ which is the closest to the temperature gradient becomes the cell growth direction [11]. The EDS point analyses suggest the intercellular network to be formed by Mo segregation (7.6±0.5 wt.% compared to 6.2±0.6 wt.% in the cells). Other works [12, 13] report on segregation of Mo together with C, however, due to the negligible C content in the initial powder used for SLM (table 2), C segregation was not observed in this work.

The XRD analysis detected 70% of HCP ε-phase and only 30% of γ-phase. Such a high amount of ε-phase can be attributed to the repeated heat affection of the already solidified material by laser melting of newly deposited layers. In combination with the preheating of the building plate, temperature can fluctuate at a high enough level for sufficiently long time to induce $\gamma \rightarrow \varepsilon$ transformation similarly to isothermal annealing below the transformation temperature [14].

3.3 Mechanical properties

Comparison between the mechanical properties of the cast and SLM Co-28Cr-6Mo alloy is shown in the bar chart in figure 5. Hardness showed to be isotropic for the whole SLM material no matter on the tested section as it is ruled by the fine cellular microstructure which does not show any directionality. The average hardness value for the SLM material was 357±3 HV10. Hardness higher by 50 units compared to the cast material can be attributed to the fine cellular microstructure with Mo segregation forming cell boundaries and to the higher content of harder HCP ε-phase. Similarly, it is with the yield and ultimate strength under both tensile and compressive loading. Yield strength showed an increase

compared to the cast material by 12-19%, ultimate tensile and compressive strength increased by 50%. Material plasticity was favourably affected by the absence of brittle secondary phases such as coarse carbide particles and continuous carbidic film on grain boundaries in the cast material.

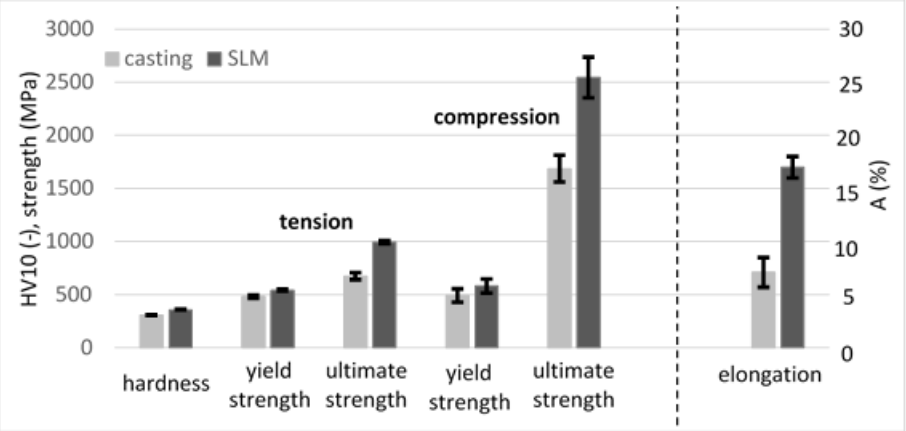

Figure 5. Mechanical properties of Co-28Cr-6Mo alloy prepared by SLM and by investment casting.

4 Conclusion

Microstructure refinement due to the rapid solidification during SLM together with the absence of secondary phases have brought increase not only in the strength but also in the plasticity of the Co-28Cr-6Mo alloy conventionally processed by investment casting. The distinctive microstructure of the additively manufactured alloy together with the detected carbon absence can be expected to be the cause of many other variances in the material behaviour, such as during heat treatment, corrosion exposition etc., which is the subject of our ongoing studies.

Acknowledgements

This work was supported from the grant of Specific university research – grant No. A2_FCHT_2020_026.

References

[1] Giacchi J V, Morando C N, Fornaro O and Palacio H A 2011 *Mater. Charact.* **62** 53-61
[2] Narushima T, Ueda K and Alfirano 2015 *Advances in Metallic Biomaterials: Tissues, Materials and Biological Reactions,* ed M Niinomi, T Narushima and M Nakai (Berlin: Springer) pp 157-178
[3] Pollock T M 2016 *Nature Mater.* **15** 809-815
[4] Arcam EBM System *ASTM F75 CoCr Alloy* http://www.arcam.com/wp-content/uploads/Arcam-ASTM-F75-Cobalt-Chrome.pdf
[5] Mergulhão M V, Podestsá C E and Neves M D M 2018 *Biomaterials in Regenerative Medicine* ed L A Dobrzański (Rijeka: InTech) chapter 6 pp 61-185
[6] Song C B, Park H B, Seong H G and López H F 2006 *Acta Biomater.* **2** 685-691
[7] López H F and Saldivar-Garcia A J 2008 *Metal. Mater. Trans.* A **39** 8-18
[8] Rosenthal R, Cardoso B R, Bott I S, Paranhos R P R and Carvalho E A 2010 *J. Mater. Sci.* **45** 4021-28
[9] Mullis A M, Farrell L, Cochrane R F and Adkins N J 2013 *Metall. Mater. Trans.* B **44** 992-999
[10] Zhang J, Song B, Wei Q, Bourell D and Shi Y 2019 *J.Mater. Sci, Technol.* **35** 270-284
[11] Chen Z W, Phan M A L and Darvish K 2017 *J. Mater. Sci.* **52** 7415-7427
[12] Song C, Zhang M, Yang Y, Wang D and Jia-kuo Y 2018 *Mater. Sci. Eng.* A **713** 206-213
[13] Li J, Ren H, Liu C and Shang S 2019 *Materials* **12** 1321
[14] Zhang M, Yang Y, Song C, Bai Y and Xiao Z 2018 *J. Alloys Compd.* **750** 878-886